Extracting the Americyl Hydration from an Americium Cationic Mixture in Solution: a Combined X-ray Absorption Spectroscopy and Molecular Dynamics Study

Sergio Pérez-Conesa, José M. Martínez, Rafael R. Pappalardo, and Enrique Sánchez Marcos*

Department of Physical Chemistry, University of Seville, 41012 Seville, Seville, Spain

E-mail: sanchez@us.es

Phone: +34 955421005

Abstract

The Am(VI) solution chemistry differs from that of lighter actinoids, as U, Pu and Np, where the actinyl $[AnO_2]^{2+}$ is the most stable form and plays an important role in nuclear fuel technology. The behavior of americium in solution shows the trend to stabilize lower oxidation states, mainly Am(III). Riddle and col. (J. Radioanal. Nuclear Chem. **2016**, *309*, 1087.) have recently reported the EXAFS and first XANES spectra of an americium-containing aqueous solution where the Americyl species is detected in a mixture. We have developed Am^{3+}-H_2O and $[AmO_2]^{2+}$-H_2O intermolecular potentials based on quantum-mechanical calculations to carry out classical MD simulations of these two cations in water. Structural information extracted from the statistical trajectories has been used to simulate EXAFS and XANES spectra of both solutions. For the Am^{3+} case the theoretical-experimental agreement for both EXAFS and XANES

spectra is satisfactory. This is not the case for the $[AmO_2]^{2+}$ aqueous solutions. However, when considering an aqueous solution mixture of both cationic forms in a 55/45 $[AmO_2]^{2+}/Am^{3+}$ ratio, the theoretical-experimental agreement is recovered. The EXAFS and XANES spectra which would correspond to a pure $[AmO_2]^{2+}$ aqueous solution are proposed. In the XANES case, the main features characterizing the simulated spectrum are consistent with those previously found in the experimental XANES spectra of stable $[UO_2]^{2+}$ and $[PuO_2]^{2+}$ in water.

Introduction

Americium is formed as a byproduct of the irradiation of uranium by neutrons as well as of Pu decay.[1] It is of great interest since it is one of the main responsible of the high radiotoxicity of minor actinoids in nuclear fuel waste.[2–4] To engineer such a waste recycling process, to understand the biological hazard of americium or to study its geochemical speciation, detailed knowledge of its complex solution chemistry is necessary. Unlike lanthanoids, the aqueous chemistry of actinoids is very rich since each element does have a distinct behaviour with different stable oxidation states and species.[5] The An(VI) solution chemistry of lighter actinoids, as U, Pu and Np, is dominated by the actinyl species, $[AnO_2]^{2+}$, which is stable and plays an important role in nuclear fuel technology. However, the behavior of Am in solution tends to stabilize lower oxidation states, mainly the Am(III), adopting the monatomic form, Am^{3+}. The stabilization of americyl species requires the presence of highly oxidizing media.[6] The ability to examine these higher oxidation states solution chemistry would yield relevant information on how these forms could be incorporated in new separation processes of minor actinoids in nuclear fuel recycling.[1–4]

Structural information on aqueous americium ionic solutions has been obtained by means of Extended X-Ray Absorption Fine Structure Spectroscopy (EXAFS).[6–9] This technique provides accurate short-range structural information around metal ions[10,11] at concentrations as low as 10^{-4} M, typical values found in actinoid solutions.[12] Unfortunately, its ra-

diotoxicity makes the experimental information about americium highly-resource demanding and scarce. Extracting information and interpreting the spectra becomes an involved task, since experimental structural information obtained from other techniques is limited, so that structural models to help in the EXAFS fitting are lacking. This leads in many cases to assumptions about the model system based on analogies with other lighter actinoids[12] or to find out synergies with theoretical tools.[13–17]

The most stable species of Am in solution is its aqua ion, $[Am(H_2O)_n]^{3+}$, whose EXAFS spectrum has been measured by Allen et al.[9] and Stumpf et al.[7,8] These studies established Am^{3+} hydration numbers in the range of 7.4-10 with an Am-O distance range of 2.477-2.494 Å. Riddle et al.[6] have very recently obtained the first EXAFS spectrum of Am(VI), $[AmO_2]^{2+}$, in a 1M HNO_3 aqueous solution containing $NaBiO_3$. These authors reported that the sample solution must be an Am(VI)/Am(III) mixture having a 70/30 ratio on the basis of UV-vis spectroscopy, although radiolysis degradation and sample stability may affect these values during the sample preparation, transportation and measuring.[6] Because of the low americium concentration (below 0.015M) in the sample we can assume that the recorded spectrum can be envisaged as a weighted sum of the two individual and independent contributions provided the absence of significant interactions among the americium ions. Thus, Riddle et al.[6] obtained structural parameters of the present species, assuming a complex model including contributions from the two oxidation states, Am(III) and Am(VI). For the americyl, these authors reported Am-O_{yl} and Am-O_I distances of 1.69 Å and 2.44 Å, respectively. These values were obtained from a fitting of a mixture solution composed by 70% of Am(VI), $\sim$ 29% of Am(III) and a marginal presence of Am(V) ($\sim$ 1%). A first-shell coordination number of 1.3 for O_{yl}, which results from the main contribution of two O_{yl} back-scatterers weighted by the percentage of americyl in the sample ($\sim$ 70%), and 4.1$\pm$0.8 which roughly results from the backscattering contribution of five oxygen atoms of the first hydration shell weighted by the same percentage of americyl in the sample were obtained. Debye-Waller factors, which reflect the structural and dynamical disorder of a given shell

of back-scatterers surrounding the metal cation, surprisingly shows smaller stiffness for the Am=O_{yl} covalent bonds than for the Am-OH_2 intermolecular bonds, 0.006 Å^2 and 0.002 Å^2, respectively, a fact difficult to rationalize. Because the EXAFS spectrum corresponds to a mixture of oxidation states as opposed to the most common EXAFS fitting scenario involving only one well-defined species as absrober, this is a challenging experiment which needs additional information to fully resolve the hydration structure of the cation mixture present in the sample.

Computational modeling of actinoids has become an interesting alternative or complement to experiment and is currently a well-established tool.[18] Nevertheless, published theoretical studies[15,17,19–22] on americium compounds in solution are scarce compared to other actinoids, although the experience from other actinoids should be partially transferable. Computation of EXAFS spectra from the structural information obtained by statistical simulations can contribute, as previously shown, to the interpretation of the experimental spectra.[13,15,17,23–25] Conversely, the agreement with experimental results supports the interaction potentials employed as well as the physicochemical properties derived from the simulation.

The aim of this work is to rationalize the experimental XAS spectra[6] of the $[AmO_2]^{2+}$ /Am^{3+} mixture in solution from a theoretical view, identifying individual contributions. For this purpose, XAS spectra will be computed from the structural information provided by MD simulations. In this case, both cations form stable aqua ions in solution, $[AmO_2(H_2O)_n]^{2+}$ and $[Am(H_2O)_m]^{3+}$, with n=5 and m=8-9. The first task is the development of specific *ab initio* interaction potentials of these cations with water. To fulfill this requirement we use our Hydrated Ion Model,[26] which is based on the assumption that the cationic reference species in solution is the aqua ion, i.e. the hydrated ion.[13,26,27] Recently we have published[16] a classical interaction potential, based on first-principles calculations, to describe uranyl in water considering the hydrated uranyl, $[UO_2(H_2O)_5]^{2+}$, instead of the naked ion $[UO_2]^{2+}$ in aqueous solution. From classical MD simulations, we were able to successfully simulate its EXAFS spectrum and investigate the hydration dynamics, structure and thermodynamics of

aqueous uranyl. The performance of this potential has been shown recently in the description of uranyl in the liquid vein of a clay.[28]

Computational Methods

The Hydrated ion model is a classical electrochemical concept developed to better describe the physicochemical properties of highly-charged metal cations.[29,30] This model recognizes the hydrated ion as the representative solute instead of the naked ion. This is necessary because the polarization exerted by the ion on its first shell is such that first-shell water molecules must be considered to be different molecular species than bulk water molecules.[31] Therefore, first-shell water molecules must have a different description than bulk water molecules and their charges and interaction potential parameters must be developed specifically for them. This imposes a restriction: the model is only applicable to hydrated ions whose first-shell residence times are longer than the simulation time. This restriction is due to the fact first-shell water release would lead to an arrangement where one or several water molecules with fitted parameters to be in the first shell are in the bulk. To get the ab initio interaction energies, all QM calculations are carried out in the presence of the full first hydration sphere. This procedure has two main advantages: the first one is completely general, it avoids the overpolarization that would occur if only one water molecule was considered to describe the ion-water interaction; the second one concerns the case of open-shell metal cations, the ion is in the correct electronic state in solution due to the presence of the ligand field provided by the hydration shell. Additional information about the Hydrated Ion Model and its extension allowing the first-shell water molecule exchange on the basis of a polarizable can be found elsewhere.[13,16,32–35]

B3LYP[36,37] reproduces reasonably well the properties of actinyl cations[38,39] treating the multireference problem in an effective way. In order to be consistent with the previous uranyl potential, the level of theory chosen for $[AmO_2(H_2O)_5]^{2+}$ was B3LYP employing the

semi-relativistic Stuttgart pseudopotential[40] with its recommended basis for americium and aug-cc-PVDZ for light atoms.[41] The americyl-pentahydrate is a quartet and B3LYP wavefunction shows low spin contamination, <S(S+1)> = 3.84 instead of 3.75, the pure-spin eigenvalue. To check the structural and energy results we have carried out a NEVPT2[42–44] computation of the americyl-hydrate including 9 electrons and 10 orbitals in the active space. Basis sets ma-def2-TZVP[45] on oxygen atom, def2-SVP[46] on hydrogen atom and DEF-TZVP[47]/SD(60,MWB) pseudopotential for Am[40] were used. Our B3LYP optimizations produce Am-O_{yl} and Am-O_I bondlengths of 1.71 Å and 2.48 Å, respectively, and an interaction energy of -226.2 kcal mol^{-1} including counterpoise correction. NEVPT2 as implemented in the ORCA program[48] provides very similar results: optimized distances of 1.75 Å and 2.42 Å for Am-O_{yl} and Am-O_I bondlengths, respectively, and an interaction energy of -239.4 kcal mol^{-1} including counterpoise correction. If the structural disagreement was substantial the simulated EXAFS, which will be presented later on, would deviate strongly from experiment. Since such is not the case, B3LYP seems an adequate computational level for the purposes of this article, i.e. to understand the nature of the Am(VI)/Am(III) mixture. The optimized geometries and interaction energies of Am(VI) at both levels of series are included in Table S1 of the Supporting Information (SI).

The method used to develop the interaction potential of uranyl,[16] which is a general strategy for any hydrated actinyl cation, was applied on the americyl-pentahydrate. The total interaction potential of an actinyl in solution within the Hydrated Ion Model, as developed for the uranyl case,[16] is the result of combining three interaction potentials: one to describe the flexibility of the actinyl molecular cation, (O=An=O), a second intermolecular potential between the actinyl and the water molecules forming the hydrate, ($[AnO_2]^{2+}$−H_2O), which defines the intrinsic dynamic of the pentahydrated actinyl, ($[AnO_2(H_2O)_5]^{2+}$) and a third intermolecular potential to describe the interaction of bulk water molecules with the actinyl hydrate, ($[AnO_2(H_2O)_5]^{2+}$ – H_2O). This implies that the model considers two types of water molecules in solution: first-shell and bulk water molecules. The intramolecular interaction

potential within the $[AmO_2]^{2+}$ hydrated ion was developed specifically for this species. The non-electrostatic interaction contribution between bulk water molecules and the hydrated ion is the same as for the uranyl case since it was found to be fairly unspecific to the actinoid (Figure S1 of the SI). The interaction potential parameters can be found in Tables S2-S6 of SI.

The level of theory chosen to develop the potential for $[Am(H_2O)_8]^{3+}$ was MP2 using the semi-relativistic pseudopotential of Sttugart,[49] which was specifically developed to treat the Am^{3+} cation, with its recommended basis set on americium and cc-PVTZ[41,50–52] on light atoms. All quantum-mechanical calculations were run with *Gaussian09*.[53] Dolg and col.[49] developed a series of specific pseudopotentials for the trivalent cations of the actinoid series, including the f-electrons in the pseudopotential. In this way the challenging issue of the f-electron open-shell is not longer found. This series of pseudopotentials is particularly convenient to deal with the actinoid hydration, as Dolg. and col.[54] showed by studying the actinoid hydration of the whole An^{3+} series with the semicontinuum model. Am^{3+}, like most large trivalent cations, must have a first-shell water mean residence time in the range 2-10 ns.[17,55] The aim of the Am^{3+}-H_2O interaction potential is to get a reasonable representation of the solution structure validated by realistic simulated EXAFS and XANES spectra. Therefore, for Am^{3+} the coordination number of the first shell was kept fixed at a given hydration number following our Hydrated Ion model.[26,34] Because the coordination number along the actinoid series is known to change from 9 to 8, we have considered both Am^{3+} hydrates, $[Am(H_2O)_m]^{3+}$ for m=8 and 9, to develop an intermolecular potential with water. This gives us a reasonable range of possible Am^{3+} hydrates in solution. The gas phase optimized Am-O distances for the octahydrate and enneahydrate are 2.51 Å and 2.56 Å, respectively. The optimized geometries and interaction energies of Am(III) with both coordination numbers are included in Table S1 of the SI. The first-shell water molecule geometry was that of the gas phase QM optimization of $[Am(H_2O)_m]^{3+}$. RESP[56] effective charges obtained from PCM[57,58] polarized wavefunction were assigned to the first-shell water molecules. The

employed water models are not polarizable and therefore polarization of the charges of the hydrated ion by the bulk solvent is included in a mean field sense with the PCM method. All water-water van der Waals interactions were described by the TIP4P[59] Lennard-Jones parameters. Additionally angular harmonic interaction potentials (O-Am-O) for first-shell oxygen atoms were incorporated. The first-shell water oxygen-metal interaction was modeled as a harmonic bonding potential. The angular and bonding harmonic interaction terms are included in order to preserve the first-shell coordination integrity. The interaction potential parameters can be found in Tables S2, S3, S7 and S8 of SI.

5 ns molecular dynamics simulations were run for each of the americium species. Simulation boxes contained the ion and 1500 water molecules including first-shell water molecules. The TIP4P[59] model was employed for bulk water molecules. The simulation ensemble was NPT at 300 K and 1 atm. The time step chosen was 1 fs and all water molecules were kept rigid. Electrostatic interactions were calculated using the Ewald Summation method with cutoff radius of 14 Å and 10^{-6} for relative error. The program used was *DL_POLY CLASSIC*.[60] Details of the simulation can be found elsewhere.[16]

Results and Discussion

Table 1 summarizes the main results of our simulations and the published experimental works. In the rest of the section we detail the our results.

Figure 1 displays the Am-O and Am-H RDFs for the simulations of Am^{3+} in water (top), which includes the results derived from the intermolecular potentials assuming the Am(III) octahydrate (solid lines) and ennea-hydrate (dashed lines), and $[AmO_2]^{2+}$ (bottom). The Am(III) hydration structure derived from the $[Am(H_2O)_8]^{3+}-H_2O$ potential is dominated by a well-defined first hydration shell with two sharp peaks centered at 2.47 Å for Am-O and 3.15 Å for Am-H pairs. The second shell is formed by 19-20 water molecules with Am-O and Am-H peaks centered at 4.64 Å and 5.21 Å, respectively. When the $[Am(H_2O)_9]^{3+}-H_2O$

Table 1: Simulation and experimental results of Am(III) and Am(VI) in solution. The properties displayed are translational self diffusion coefficient (D_i),[61] hydration enthalpy (ΔH_{hydr}),[30] metal-oxygen distances (r),[7–9] coordination numbers (CN)[7–9] and Debye-Waller factors (DW).[7–9]

	$[AmO_2{\cdot}(H_2O)_5]^{2+}$		$[Am{\cdot}(H_2O)_n]^{3+}$		
	MD	Exp.	MD $n=8$	MD $n=9$	Exp.
D_iÂů10^5 ($cm^2\ s^{-1}$)	1.3 ± 0.1	∼	0.7 ± 0.2	0.8 ± 0.2	0.625 ± 0.003
ΔH_{hydr}, ($kcal\,mol^{-1}$)	-342	∼-325,∼-401	-870	-886	-823
r(Am-O_{yl}), (Å)	1.72	1.69	-	-	-
CN(Am-O_{yl})	2*	1.3	-	-	-
DW(Am-O_{yl}), ($Å^2$)	0.007	0.006	-	-	-
r(Am-O_I), (Å)	2.44	2.48	2.47	2.53	2.473
CN(Am-O_I)	5*	4.1	8*	9*	7.4, 8.4, 10
r(Am-O_{II}), (Å)	4.64	-	4.66	4.72	2.473
CN(Am-O_{II})	29*	-	19	19	-
DW(Am-O_I), ($Å^2$)	0.007	0.002	0.006	0.007	0.007, 0.009

*Fixed.

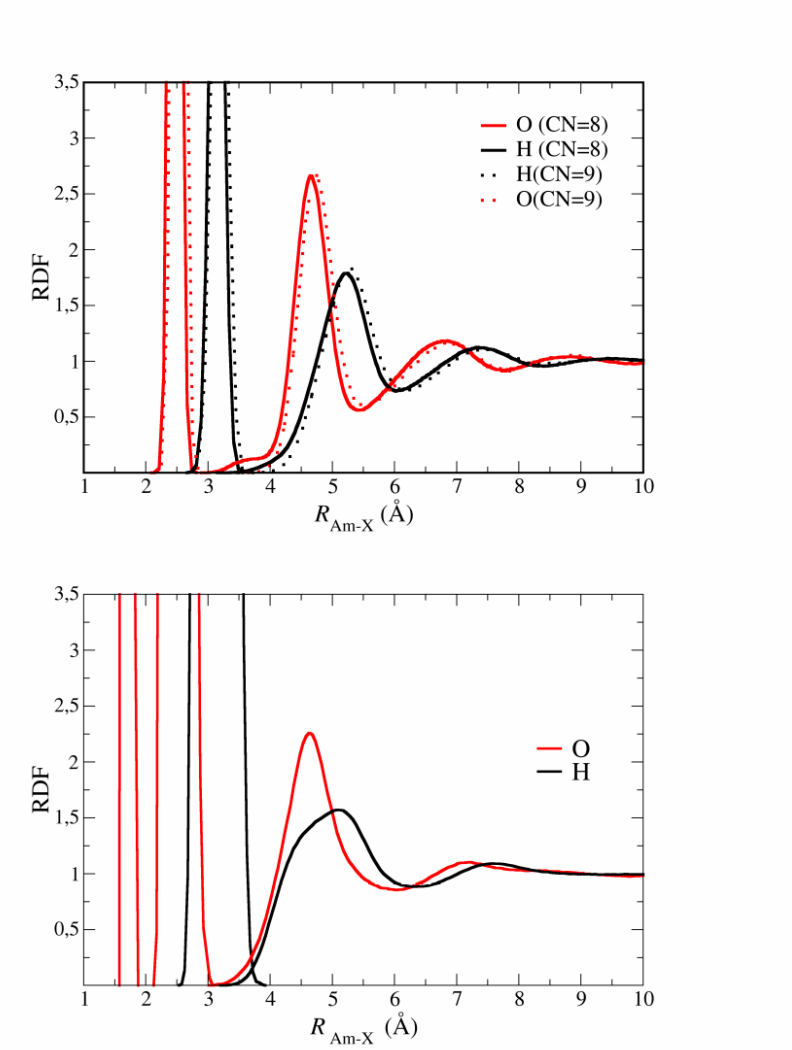

Figure 1: Am-O and Am-H RDFs for Am^{3+} (top) and $[AmO_2]^{2+}$ (bottom) aqueous solutions derived from MD simulations.

potential is employed, as expected, it is observed an Am-water lengthening, thus the two first Am-O peaks are centered at 2.53 Å and 4.74 Å, and a similar shifting for the Am-H peaks. In the americyl case, Am-O RDF (Figure 1 bottom) shows a sharp peak centered at 1.72 Å and integrating to two, which corresponds to the O_{yl} atoms. A second well-defined peak, broader than the previous one, is centered at ∼2.45 Å and integrates to five. This is the equatorial hydration shell of the americyl cation. A third Am-O peak centered at 4.64 Å and integrating to ∼30 collects the second-shell water molecules of the equatorial region together with water molecules solvating the axial and the intermediate region between that and the equatorial one. This complex combination of hydrating water molecules around the Americyl pentahydrate is also reflected in the Am-H RDF. The second Am-H peak overlaps with the Am-O ones. This indicates the different orientations of water molecules in the axial, equatorial and intermediate regions. This complex hydration structure was already observed in the $[UO_2]^{2+}$ case and we refer to that work for a deeper description of this hydration structure based on angle-solved RDFs,[16] as well as to the analysis carried out by Maginn's group.[20,21] Figures S2 and S3 of SI plot the angle-solved RDFs for americyl penta-hydrate.

To calculate the Am^{3+} hydration enthalpy, $\Delta H^{\text{theor}}_{\text{hydr}}$ (Am^{3+}), we have computed two contributions:

$$\Delta H^{\text{theor}}_{\text{hydr}}(Am^{3+}) = \Delta H^{\text{MD}}_{\text{hydr}}([Am(H_2O)_8]^{3+}_{\text{aq}}) + \Delta H^{\text{QM}}_{\text{form}}([Am(H_2O)_8]^{3+})$$

The first one is the hydration enthalpy of the $[Am(H_2O)_8]^{3+}$ aqua ion in water that is computed from MD simulations of the Am^{3+} aqua ion in water, pure water and the aquaion in gas phase at the same temperature:

$$\Delta H^{\text{MD}}_{\text{hydr}}([Am(H_2O)_8]^{3+}_{\text{aq}}) = H^{\text{MD}}([Am(H_2O)_8]^{3+}\text{in water}) - H^{\text{MD}}(\text{water}) - H^{\text{MD}}([Am(H_2O)_8]^{3+})$$

The second contribution corresponds to the formation enthalpy of the $[Am(H_2O)_8]^{3+}$ aqua ion. This is computed at the quantum-mechanical level used to build the potential energy surface which was employed further to generate the Am^{3+}-water intermolecular potential. Thermal corrections were included using the ideal gas rotational and translational partition functions at 300 K. The zero point energy was included using the harmonic oscillator model. The relaxation energy of water molecules from gas phase to solution was neglected since it is very small in comparison to ΔH_{hydr}.

$$\Delta H^{\mathrm{QM}}_{\mathrm{form}}([Am(H_2O)_8]^{3+}) = H^{\mathrm{QM}}([Am(H_2O)_8]^{3+}) - H^{\mathrm{QM}}(Am^{3+}) - 8 \cdot H^{\mathrm{QM}}(H_2O).$$

The theoretical hydration enthalpy for Am(III) is -870 kcal mol^{-1} that agrees reasonably with the experimental estimation of -823 kcal mol^{-1} (6% relative error),[30] bearing in mind the typical uncertainty of ionic hydration for highly-charged cations, and particularly for heavy actinoids.[30] Martelli et al.[62] from their classical MD simulation of Am^{3+} obtained a value of -869±11 kcal mol^{-1}, that matches the value obtained in this work. When considering the case of the ennea-hydrate, the estimated hydration enthalpy for Am(III) is -886 kcal mol^{-1}.

There is no experimental hydration enthalpy for $[AmO_2]^{2+}$, but there are estimations for other lighter actinyls based on empirical models which range between -325±5 and -401±15 kcal mol^{-1}.[63,64] We computed the $[AmO_2]^{2+}$ hydration enthalpy as the difference between the enthalpies derived from MD simulations of $[AmO_2]^{2+}$ in water and that of the sum of the TIP4P bulk water and $[AmO_2]^{2+}$ in gas phase.

$$\begin{aligned}\Delta H^{\mathrm{theor}}_{\mathrm{hydr}}([AmO_2]^{2+}_{\mathrm{aq}}) = {} & H^{\mathrm{MD}}([AmO_2]^{2+}\text{in water}) \\ & - H^{\mathrm{MD}}(\text{water}) - H^{\mathrm{MD}}([AmO_2]^{2+})\end{aligned}$$

The theoretical estimation is -342±16 kcal mol^{-1} what is consistent with the estimation from empirical models.[63,64]

Regarding the dynamics of the cations, self-translational diffusion coefficient has been

computed from their MD trajectories as done in a previous work.[16] Their D_i finite-size corrected[65] are $1.3 \pm 0.1 \cdot 10^{-5}$ cm^2 s^{-1} for $[AmO_2]^{2+}$, $0.7 \pm 0.2 \cdot 10^{-5}$ cm^2 s^{-1} for $[Am(H_2O)_8]^{3+}$ and $0.8 \pm 0.2 \cdot 10^{-5}$ cm^2 s^{-1} for $[Am(H_2O)_9]^{3+}$. The experimental diffusion coefficient[61] of Am^{3+} is $0.625 \pm 0.003 \cdot 10^{-5}$ cm^2 s^{-1} which agrees within the statistical uncertainty with our estimation. Martelli et al.[62] have computed from classical MD simulations that used a polarizable interaction potential, the diffusion coefficient of Am^{3+}, $0.63 \pm 0.2 \cdot 10^{-5}$ cm^2 s^{-1}. The diffusion coefficient of $[AmO_2]^{2+}$ is similar to our result for $[UO_2]^{2+}$ as can be expected by the physicochemical similarity of these two species.[16] To the best of our knowledge, the diffusion coefficient of Am(VI) has not been published. In any case, the value obtained for Am(VI), as expected, resembles our U(VI) value[16] of $1.2 \pm 0.1 \cdot 10^{-5}$ cm^2 s^{-1}. The comparison of the diffusion coefficient of our actinyl model with experiments has been previously discussed.[16] To understand these results we must realize that the diffusional behavior of these cations is mediated by their hydrated ions rather than by their bare ions. Then, the hydrates of $[AmO_2]^{2+}$ and Am^{3+} are the real species determining the ion mobility in aqueous solution. Am^{3+} hydrate is of similar size to the $[AmO_2]^{2+}$ hydrate, but its higher charge justifies its smaller diffusion coefficient value.

The Am L_3-edge EXAFS and XANES spectra were computed as the average of the individual spectra of 500 snapshots evenly taken from the MD trajectories. The spectra were obtained using FEFF9.6.[66,67] (examples of FEFF input files are included in the SI). These snapshots included two hydration shells. EXAFS spectra include multiple scattering paths up to 4 legs and XANES spectra full multiple scattering contributions. To simulate the spectrum of the $[AmO_2]^{2+}$/Am^{3+} mixture, the individual spectra were summed using the weighting factor of each oxidation state.

Figure 2 (top) shows the comparison of the experimental k^2-weighted Am L_3-edge of an acidic aqueous Am(III) solution (black dashed line) recorded by Stumpf et al.[7] and the simulated spectrum derived from our $[Am(H_2O)_8]^{3+}$ MD simulation (green line). The shape of the experimental EXAFS signal indicates a rather simple contribution, mainly due to the

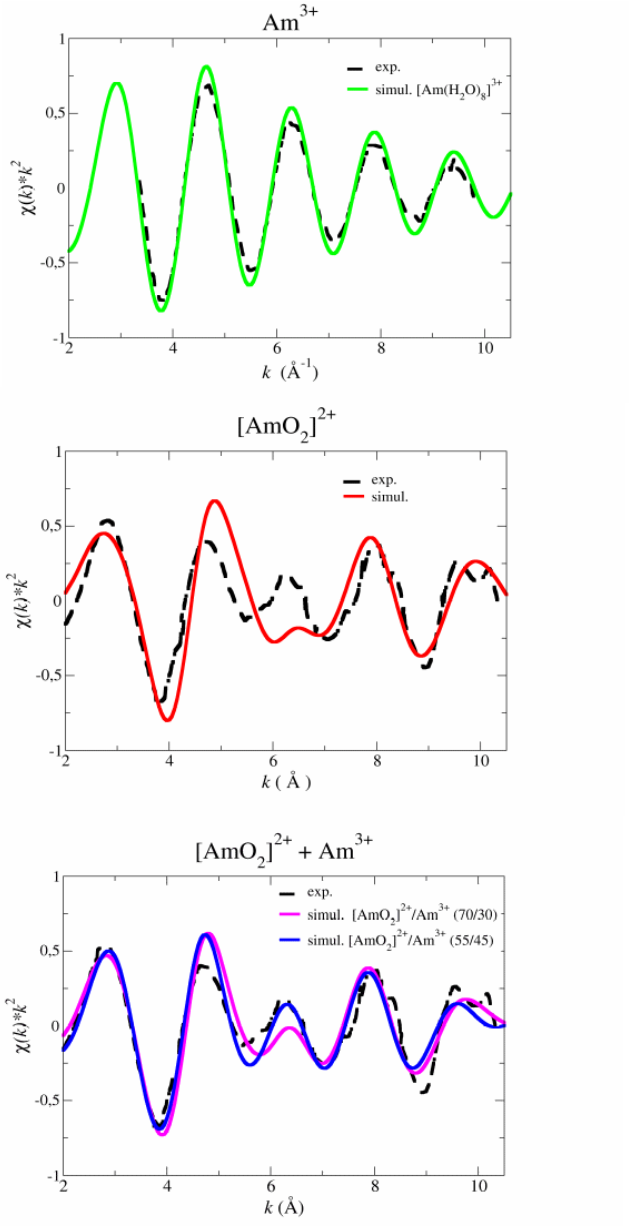

Figure 2: Experimental (dashed lines) vs. simulated (solid lines) Am L_3-edge k^2-weighted EXAFS spectra. Top: experimental (ref.[7]) and simulated Am^{3+} aqueous solution; Middle: experimental Am ionic mixture (ref.[6]) and simulated spectrum of $[AmO_2]^{2+}$ (red line); Bottom: experimental Am ionic mixture (ref.[6] and simulated spectra with the 70/30 (magenta line) and a 55/45 (blue line) ($[AmO_2]^{2+}/Am^{3+}$) ratios.

single scattering paths of the first-hydration shell water molecules. The simulated spectrum (green line) reproduces pretty well the frequency and intensity of the signal. This agreement allows the assignment of an octa-coordination for A m(III) with a first-shell Am-O distance of 2.47 Å and a DW factor for the first hydration shell of 0.0055 $Å^2$. An analogous simulated EXAFS spectrum was carried out from the MD simulation containing the ennea-hydrated Am(III). The comparison between the Am(III) EXAFS spectra of the two coordination numbers with the experimental one is given in Figure S4 (top) of the SI. The difference in the EXAFS is noticeable since the change in coordination and M-O distance has a strong impact in the EXAFS. A similar or larger discrepancy for the CN=7.4 and 10 must be expected.

Stumpf et al.[7,8] and Allen et al.[9] from their experimental EXAFS analysis obtained the same Am-O distance, 2.48 Å, and coordination numbers of 7.4 and 10, respectively. DW factors of 0.0069 and 0.0090 $Å^2$, respectively, were fixed in the fitting. Spezia et al.[15,17] have studied the Am(III) by means of two approaches, revisiting the EXAFS analysis and from MD simulations, obtaining Am-O distances in the range 2.47-2.49 Å, although they found an ennea-coordination. These authors also obtained a fair agreement between the experimental spectrum and that simulated. As they pointed out, the ± 1 uncertainty in coordination numbers for aqua ions is intrinsic to EXAFS spectroscopy.

Figure 2 (middle) plots the experimental EXAFS spectrum recorded by Riddle and col.[6] of an aqueous solution (black dashed line) containing several Am cationic forms, americyl being the most abundant one. The simulated EXAFS spectrum corresponding to a pure sample of $[AmO_2]^{2+}$ in water (red line) is also in the same figure. Both signals are complex, indicating several contributions out of phase with different intensities. This might be inherent to the $[AmO_2(H_2O)_5]^{2+}$ species, where there are contributions from Am=O_{yl} and Am-O_I paths with quite different distances. DW factors computed from our MD simulations are 0.00074 $Å^2$ for Am-O_{yl} and 0.0072 $Å^2$ for Am-O_I. Both factors may justify such a peculiar EXAFS spectrum shape. However, the agreement between the experimental and simulated

spectra is not satisfactory. As suggested by Riddle et al.[6] the relative instability of the Am(VI) oxidation state leads to a mixture of Am(VI) and Am(III) in the solution and a marginal presence of Am(V). Figure 2 (bottom) shows the comparison of the experimental (dashed black line) with the theoretical spectra (blue and magenta lines) obtained from two different weighted sums of the Am^{3+} and $[AmO_2]^{2+}$ simulated spectra shown in the two upper plots. The much better agreement gives evidence for the presence of an Am cationic mixture in the aqueous solutions recorded by Riddle et al.[6] In our case, the best $[AmO_2]^{2+}/Am^{3+}$ ratio matching as much as possible the experimental signal was achieved with a 55/45 value (blue line), whereas the suggested experimental value was 70/30 (magenta line). Although both ratios give simulated spectra similar to the experimental one, our proposed ratio performs better. The observed discrepancy of ratios is probably a consequence of the uncertainty in both the theoretical procedure and the experimental determination of the Am species concentration in the measured sample. The MD simulation used for the Am^{3+} contribution to the simulated spectrum was that using the $[Am(H_2O)_8]^{3+}$ hydrate. The comparison of the experimental results with the simulated spectrum obtained using the Am(III) ennea-hydrate MD simulation is plotted in Figure S4 of SI (bottom). It is clear the better theoretical-experimental agreement derived from the use of the Am(III) octahydrate EXAFS spectrum. Two conclusions can be derived from the analysis of Figure 2 and Figure S4 of SI. The first one is that, even though the high oxidizing character of the medium, the experimental spectrum clearly is the combination of the two Am cationic species regardless the cation ratio applied and the Am(III) hydrate selected to combine. The second conlusion is that the best agreement obtained with a different cation ratio to that experimentally proposed, but not too far, suggests some uncertainty in the individual Am species population really present in the measured sample. As a consequence of this analysis we can establish that the simulated EXAFS spectrum (red line) in the middle of Figure 2 is our theoretical proposal for the spectrum of an $[AmO_2]^{2+}$ dilute aqueous solution.

An additional test on the cationic mixture aqueous solution can be made by the theoretical-

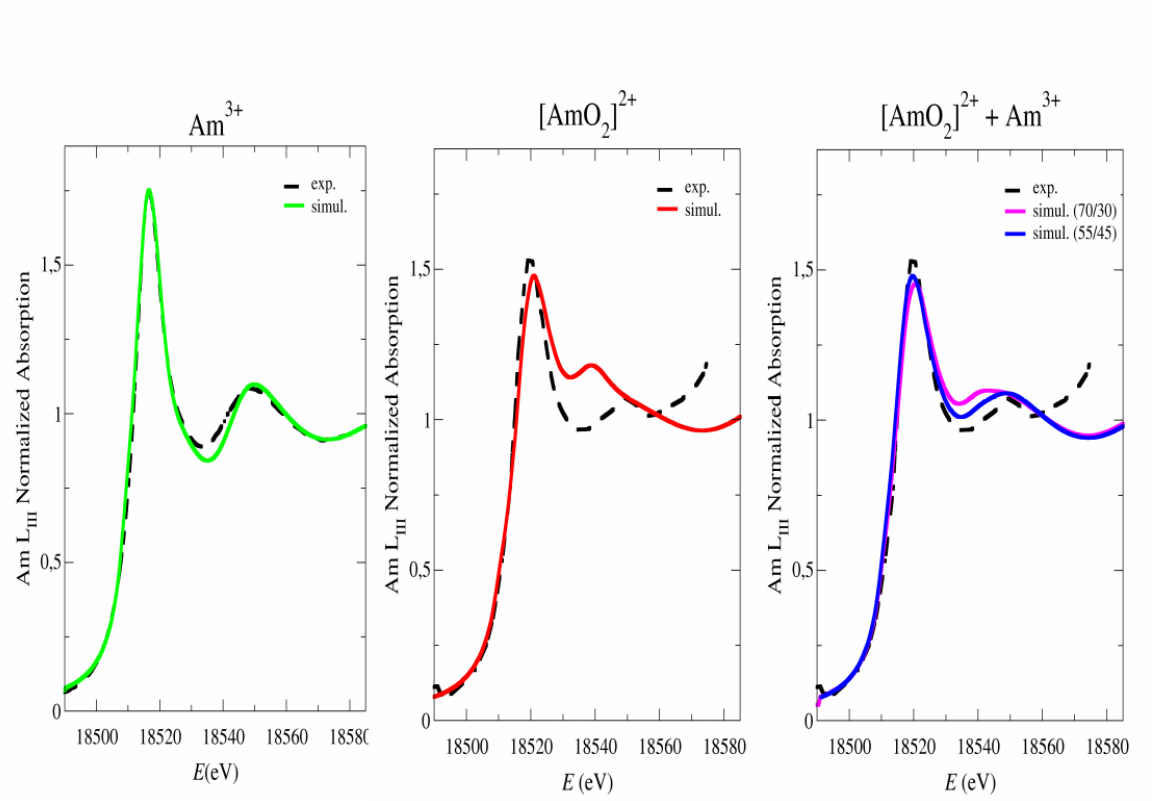

Figure 3: Experimental (dashed lines) vs. simulated (solid lines) Am L_3-edge k^2-weighted XANES spectra. Top: experimental (ref.[7]) and simulated Am^{3+} aqueous solution; Middle: experimental Am ionic mixture (ref.[6]) and simulated spectrum of $[AmO_2]^{2+}$ (red line); Bottom: experimental Am ionic mixture (ref.[6] and simulated spectra with the 70/30 (magenta line) and a 55/45 (blue line) ($[AmO_2]^{2+}$ /Am^{3+}) ratios.

experimental comparison of the XANES spectra of the same samples. Figure 3 displays such test for the Am(III) sample (left part) and Am(VI) sample (middle part). The agreement between the experiment (black dashed line) and the theoretical model using the $[Am(H_2O)_8]^{3+}$ (green line) is remarkable. On the contrary, there is a poor agreement of the experimental XANES (black dashed line in the center part) of the sample containing the Am(VI) oxidation state and the simulated spectrum derived from the pure $[AmO_2]^{2+}$ MD simulation. However, when the spectrum is computed considering the $[AmO_2]^{2+}/Am^{3+}$ mixture, the agreement is clearly improved. Again the 55/45 ratio (blue line in the right part of Figure 3) performs better than the 70/30 experimental proposal (magenta line). If we accept that this satisfactory result is not a consequence of fortuitous error cancellations, the model suggests that the experimental ratio of the mixture might be reconsidered. Furthermore, as in the EXAFS case, we propose the red line in the center of Figure 3 as the XANES spectrum of a pure sample of $[AmO_2]^{2+}$ in water, something that up to the present has not been measured. The larger stability of higher oxidation states in water for $[UO_2]^{2+}$ and $[PuO_2]^{2+}$ allows the experimental determination of the XANES for aqueous solutions only containing those actinyls.[68,69] The energy gap between the white line and the first resonance is $\sim$ 18 and $\sim$ 21 eV for $[UO_2]^{2+}$ and $[PuO_2]^{2+}$ XANES spectra, respectively. In the case of our simulated pure $[AmO_2]^{2+}$ aqueous solution this gap is 23 eV, what corroborates the global consistency among experimental and theoretical results. It is interesting to point out that this gap in the experimental spectrum of the mixture is $\sim$ 30 eV. The energy position of the edge in XANES has long been used as a semi-quantitative index on the absorber atom oxidation state. For systems with O atoms in the first hydration shell there is a linear correlation between the oxidation state and the edge energy, with an increase of $\sim$1.5 eV per formal oxidation state.[70] FEFF9.6 computations of the XANES spectra of aqueous solutions of the Am(III) and Am(VI) oxidation states (left:green line, and middle:red line in Figure 3) predicts 4.0 eV to compare with the empirically estimated of 4.5 eV. However, when analyzing the experimental XANES spectra (dashed lines on Figure 3, left:Am(III), middle or

right:Am(VI)) the difference is 2.0 eV whereas the value from the theoretical XANES spectra of Am(III) (left:green line) and the cationic mixture (right:blue line) is 2.5 eV.

In conclusion, this study has established a spectroscopical-theoretical procedure to deal with an aqueous solution mixture of two americium cations, Am^{3+} and $[AmO_2]^{2+}$ which contribute separately to a sole X-ray absorption spectrum. From this global experimental signal, the individual contributions to the XANES and EXAFS spectra corresponding to the pure aqueous solutions of each individual ionic species is achieved based on reliable intermolecular potentials and ab initio methods of multiple scattering theory. Discarding error cancellations, if the sum of the two contributions leads to a fair agreement with experiment, we could assume as correct the individual contributions and consequently to support the simulated EXAFS and XANES spectra of $[AmO_2]^{2+}$ as the expected Am L_3-edge spectra of a pure $[AmO_2]^{2+}$ aqueous solution. This may be envisaged as a challenge for new experiments intended to design appropriate medium conditions to stabilize selectively the $[AmO_2]^{2+}$ species in water. The combined experimental-theoretical strategy opens possibilities to the analysis of complex mixtures solutions of species containing a particular absorber atom present in different oxidation states.

Acknowledgement

We would like to thank Prof. Steven Conradson for providing us some of the experimental spectra. This work was financially supported by Consejeria de Economia, Innovacion, Ciencia y Desarrollo, Junta de Andalucía of Spain (Proyecto de Excelencia, P11-FQM7607) and the Spanish Ministry of Education, Culture and Sports for the PhD scholarship FPU (Formación de Profesorado Universitario).

Supporting Information Available

The Supporting Information is available free of charge on the ACS Publications website at DOI:

Cartesian coordinates of optimized structures of $[Am(H_2O)_8]^{3+}$, $[Am(H_2O)_9]^{3+}$ and AmO_2^{2+}, EXAFS and XANES FEFF input files, Figure comparing interaction energy scans of a bulk water molecule with $[AmO_2(H_2O)_5]^{2+}$ given by DFT and the developed classical potential, gas phase quantum-mechanical optimized geometries of the Am^{3+} and $[AmO_2]^{2+}$ hydrates, interaction potential parameters, angle-solved RDFs, theoretical-experimental comparison of the EXAFS spectrum corresponding to: (Top) simulated spectra built from $[Am(H_2O)_8]^{3+}$ and $[Am(H_2O)_9]^{3+}$ MD simulations, (Bottom) simulated spectra built with the 55/45 ratio using for Am(III) the $[Am(H_2O)_9]^{3+}$ MD simulation.

References

(1) Runde, R. W.; Schulz, W. W. In *The Chemistry of the Actinide and Transactinide Elements*, 3rd ed.; Morss, L. R., Edelstein, N., Fuger, J., Katz, J. J., Eds.; Springer, 2008; Vol. 2; Chapter 8, pp 1265–1395.

(2) Morimoto, K.; Kato, M.; Uno, H.; Hanari, A.; Tamura, T.; Sugata, H.; Sunaoshi, T.; Kono, S. Preparation and Characterization of (Pu, U, Np, Am, simulated FP)O_{2-x}. *J. Phys. Chem. Solids* **2005**, *66*, 634–638.

(3) Yoshimochi, H.; Nemoto, M.; Mondo, K.; Koyama, S.; Namekawa, T. Fabrication Technology for MOX Fuel Containing AmO_2 by an in-Cell Remote Process. *J. Nucl. Sci. Technol.* **2004**, *41*, 850–856.

(4) Prieur, D.; Carvajal-Nunez, U.; Vitova, T.; Somers, J. Local and Electronic Structure of Americium-Bearing PuO2. *Eur. J. Inorg. Chem.* **2013**, *2013*, 1518–1524.

(5) Choppin, G. R.; Jensen, M. P. In *The Chemistry of the Actinide and Transactinide Elements*, 3rd ed.; Morss, L. R., Edelstein, N., Fuger, J., Katz, J. J., Eds.; Springer, 2008; Vol. 4; Chapter 23, pp 2524–2621.

(6) Riddle, C.; Czerwinski, K.; Kim, E.; Paviet, P.; Weck, P.; Poineau, F.; Conradson, S. Characterization of Pentavalent and Hexavalent Americium Complexes in Nitric Acid Using X-Ray Absorption Fine Structure Spectroscopy and First-Principles Modeling. *J. Radioanal. Nucl. Chem.* **2016**, *309*, 1087–1095.

(7) Stumpf, S.; Stumpf, T.; Dardenne, K.; Hennig, C.; Foerstendorf, H.; Klenze, R.; Fanghänel, T. Sorption of Am (III) Onto 6-Line-Ferrihydrite and its Alteration Products: Investigations by EXAFS. *Environ. Sci. Techn.* **2006**, *40*, 3522–3528.

(8) Stumpf, T.; Hennig, C.; Bauer, A.; Denecke, M. A.; Fanghänel, T. An EXAFS and TRLFS Study of the Sorption of Trivalent Actinides Onto Smectite and Kaolinite. *Radiochim. Acta* **2004**, *92*, 133–138.

(9) Allen, P.; Bucher, J.; Shuh, D.; Edelstein, N.; Craig, I. Coordination Chemistry of Trivalent Lanthanide and Actinide Ions in Dilute and Concentrated Chloride Solutions. *Inorg. Chem.* **2000**, *39*, 595–601.

(10) Koningsberger, D.; Prins, R. *X-ray Absorption: Principles, Applications, Techniques of EXAFS, SEXAFS, and XANES*; John Wiley and Sons: New York, NY, 1988.

(11) Muñoz-Páez, A.; Sánchez Marcos, E. In *Comprehensive Inorganic Chemistry II: From Elements to Applications*, 2nd ed.; Reedijk, J., Poeppelmeier, K., Eds.; Elsevier, 2013; Vol. 9; pp 133–159.

(12) Denecke, M. A. Actinide Speciation Using X-Ray Absorption Fine Structure Spectroscopy. *Coord. Chem. Rev.* **2006**, *250*, 730–754.

(13) Galbis, E.; Hernández-Cobos, J.; den Auwer, C.; Le Naour, C.; Guillaumont, D.; Simoni, E.; Pappalardo, R. R.; Sánchez Marcos, E. Solving the Hydration Structure of the Heaviest Actinide Aqua Ion Known: The Californium (III) Case. *Angew. Chem. Int. Ed.* **2010**, *122*, 3899–3903.

(14) Atta-Fyn, R.; Bylaska, E. J.; Schenter, G. K.; de Jong, W. A. Hydration Shell Structure and Dynamics of Curium(III) in Aqueous Solution: First Principles and Empirical Studies. *J. Phys. Chem. A* **2011**, *115*, 4665–4677.

(15) D'Angelo, P.; Martelli, F.; Spezia, R.; Filipponi, A.; Denecke, M. A. Hydration Properties and Ionic Radii of Actinide (III) Ions in Aqueous Solution. *Inorg. Chem.* **2013**, *52*, 10318–10324.

(16) Pérez-Conesa, S.; Torrico, F.; Martínez, J. M.; Pappalardo, R. R.; Sánchez Marcos, E. a Hydrated Ion Model of $[UO_2]^{2+}$ in Water: Structure, Dynamics, and Spectroscopy from Classical Molecular Dynamics. *J. Chem. Phys.* **2016**, *145*, 224502.

(17) Spezia, R.; Migliorati, V.; D'Angelo, P. On the Development of Polarizable and Lennard-Jones Force Fields to Study Hydration Structure and Dynamics of Actinide(III) Ions Based on Effective Ionic Radii. *J. Chem. Phys.* **2017**, *147*, 161707.

(18) Dolg, M. *Computational Methods in Lanthanide and Actinide Chemistry*; John Wiley & Sons: University of Cologne, Germany, 2015.

(19) Vallet, V.; Privalov, T.; Wahlgren, U.; Grenthe, I. The Mechanism of Water Exchange in $AmO_2(H_2O)_5^{2+}$ and in the Isoelectronic $UO_2(H_2O)_5^{2+}$ and $NpO_2(H_2O)_5^{2+}$ Complexes as Studied by Quantum Chemical Methods. *J. Am. Chem. Soc.* **2004**, *126*, 7766–7767.

(20) Pomogaev, V.; Tiwari, S. P.; Rai, N.; Goff, G. S.; Runde, W.; Schneider, W. F.; Maginn, E. J. Development and Application of Effective Pairwise Potentials for UO_2^{n+}, NpO_2^{n+}, PuO_2^{n+}, and AmO_2^{n+} (n= 1, 2) Ions With Water. *Phys. Chem. Chem. Phys.* **2013**, *15*, 15954–15963.

(21) Tiwari, S. P.; Rai, N.; Maginn, E. J. Dynamics of Actinyl Ions in Water: A Molecular Dynamics Simulation Study. *Phys. Chem. Chem. Phys.* **2014**, *16*, 8060–8069.

(22) Fabrizio, A.; Rotzinger, F. P. Quantum Chemical Study of the Water Exchange Mechanism of the Americyl (VI) Aqua Ion. *Inorg. Chem.* **2016**, *55*, 11147–11152.

(23) Filipponi, A.; D'Angelo, P.; Pavel, N. V.; Di Cicco, A. Triplet Correlations in the Hydration Shell of Aquaions. *Chem. Phys. Lett.* **1994**, *225*, 150–155.

(24) Palmer, B. J.; Pfund, D. M.; Fulton, J. L. Direct Modeling of EXAFS Spectra from Molecular Dynamics Simulations. *J. Phys. Chem.* **1996**, *100*, 13393–13398.

(25) Merkling, P. J.; Muñoz-Páez, A.; Sánchez Marcos, E. Exploring the Capabilities of X-Ray Absorption Spectroscopy for Determining the Structure of Electrolyte Solutions: Computed Spectra for Cr^{3+} or Rh^{3+} in Water Based on Molecular Dynamics. *J. Am. Chem. Soc.* **2002**, *124*, 10911–10920.

(26) Martínez, J. M.; Pappalardo, R. R.; Sánchez Marcos, E. First-Principles Ion-Water Interaction Potentials for Highly Charged Monoatomic Cations.Computer Simulations of Al^{3+}, Mg^{2+} and Be^{2+}. *J. Am. Chem. Soc.* **1999**, *121*, 3175–3184.

(27) Morales Negrito, N. Estudio Teórico de Propiedades Fisicoquímicas de Cationes Metálicos En Disolución: Evolución en el Grupo de los Alcalinos y en la Serie de los Lantánidos. Ph.D. thesis, Universidad de Sevilla, Spain, 2015.

(28) Pérez-Conesa, S.; Martínez, J. M.; Sánchez Marcos, E. Hydration and Diffusion Mechanism of Uranyl in Montmorillonite Clay: Molecular Dynamics Using an Ab Initio Potential. *J. Phys. Chem. C* **2017**, *121*, 27437–27444.

(29) Frank, H. S.; Evans, M. W. Free Volume and Entropy in Condensed Systems III. *J. Chem. Phys.* **1945**, *13*, 507–532.

(30) Marcus, Y. *Ions in Solution and their Solvation*; John Wiley and Sons, 2015; pp 107–116.

(31) Taube, H. Use of Oxygen Isotope Effects in Study of Hydration of Ions. *J. Phys. Chem.* **1954**, *58*, 523–528.

(32) Pappalardo, R. R.; Sánchez Marcos, E. Recovering the concept of the hydrated ion for modeling ionic solutions: a Monte Carlo study of zinc(2+) in water. *J. Phys. Chem.* **1993**, *97*, 4500–4504.

(33) Pappalardo, R. R.; Martínez, J. M.; Sánchez Marcos, E. Application of the Hydrated Ion Concept for Modeling Aqueous Solutions Containing Highly Charged Ions: A Monte Carlo Simulation of Cr3+ in Water Using an ab Initio Intermolecular Potential. *J. Phys. Chem.* **1996**, *100*, 11748–11754.

(34) Martínez, J. M.; Pappalardo, R. R.; Sánchez Marcos, E.; Refson, K.; Díaz-Moreno, S.; A., M. Dynamics of a Highly Charged Ion in Aqueous Solutions : Molecular Dynamics Simulations of Dilute $CrCl_3$ Aqueous Solutions Using Interaction Potentials Based on the Hydrated Ion Concept. *J Phys Chem B* **1998**, *102*, 3272–3282.

(35) Galbis, E.; Hernández-Cobos, J.; Pappalardo, R.; Sanchez Marcos, E. Collecting High-order Interactions in an Effective Pairwise Intermolecular Potential Using the Hydrated Ion Concept: The Hydration of Cf(III). *J. Chem. Phys.* **2014**, *140*, 214104–(1)–(11).

(36) Becke, A. D. Density-Functional Thermochemistry. III. The Role of Exact Exchange. *J. Chem. Phys.* **1993**, *98*, 5648–5652.

(37) Stephens, P. J.; Devlin, F. J.; Chabalowski, C. F.; Frisch, M. J. Ab Initio Calculation of Vibrational Absorption and Circular Dichroism Spectra Using Density Functional Force Fields. *J. Phys. Chem.* **1994**, *98*, 11623–11627.

(38) Clavaguéra-Sarrio, C.; Vallet, V.; Maynau, D.; Marsden, C. J. Can Density Functional Methods Be Used for Open-Shell Actinide Molecules? Comparison With Multiconfigurational Spin-Orbit Studies. *J. Chem. Phys.* **2004**, *121*, 5312–5321.

(39) Averkiev, B. B.; Mantina, M.; Valero, R.; Infante, I.; Kovacs, A.; Truhlar, D. G.; Gagliardi, L. How Accurate are Electronic Structure Methods for Actinoid Chemistry? *Theor. Chem. Acc.* **2011**, *129*, 657–666.

(40) Küchle, W.; Dolg, M.; Stoll, H.; Preuss, J. Energy-Adjusted Pseudopotentials for the Actinides. Parameter Sets and Test Calculations for Thorium and Thorium Monoxide. *J. Chem. Phys.* **1994**, *100*, 7535–7542.

(41) Kendall, R. A.; Dunning Jr., T. H.; Harrison, R. J. Electron Affinities of the First-Row Atoms Revisited. Systematic Basis Sets and Wave Functions. *J. Chem. Phys.* **1992**, *96*, 6796–6806.

(42) Angeli, C.; Cimiraglia, R.; Malrieu, J.-P. N-electron valence state perturbation theory: a fast implementation of the strongly contracted variant. *Chem. Phys. Lett.* **2001**, *350*, 297–305.

(43) Angeli, C.; Cimiraglia, R.; Malrieu, J.-P. n-electron valence state perturbation theory: A spinless formulation and an efficient implementation of the strongly contracted and of the partially contracted variants. *J. Chem. Phys.* **2002**, *117*, 9138–9153.

(44) Jung, J.; Atanasov, M.; Neese, F. Ab Initio Ligand-Field Theory Analysis and Covalency Trends in Actinide and Lanthanide Free Ions and Octahedral Complexes. *Inorg. Chem.* **2017**, *56*, 8802–8816.

(45) Zheng, J.; Xu, X.; Truhlar, D. G. Minimally augmented Karlsruhe basis sets. *Theoretical Chemistry Accounts* **2011**, *128*, 295–305.

(46) Weigend, F.; Ahlrichs, R. Balanced basis sets of split valence, triple zeta valence and quadruple zeta valence quality for H to Rn: Design and assessment of accuracy. *Physical Chemistry Chemical Physics* **2005**, *7*, 3297–3305.

(47) Eichkorn, K.; Weigend, F.; Treutler, O.; Ahlrichs, R. Auxiliary basis sets for main row atoms and transition metals and their use to approximate Coulomb potentials. *Theoretical Chemistry Accounts: Theory, Computation, and Modeling (Theoretica Chimica Acta)* **1997**, *97*, 119–124.

(48) Neese, F. The ORCA program system. *Wiley Interdiscip. Rev. Comput. Mol. Sci.* **2012**, *2*, 73–78.

(49) Moritz, A.; Cao, X.; Dolg, M. Quasirelativistic Energy-Consistent 5f-In-Core Pseudopotentials for Trivalent Actinide Elements. *Theor. Chem. Acc.* **2007**, *117*, 473–481.

(50) Dunning Jr., T. H. Gaussian Basis Sets for Use in Correlated Molecular Calculations. I. the Atoms Boron Through Neon and Hydrogen. *J. Chem. Phys.* **1989**, *90*, 1007–1023.

(51) Woon, D. E.; Dunning Jr., T. H. Gaussian Basis Sets for Use in Correlated Molecular Calculations. III. the Atoms Aluminum Through Argon. *J. Chem. Phys.* **1993**, *98*, 1358–1371.

(52) Woon, D. E.; Dunning Jr., T. H. Gaussian Basis Sets for Use in Correlated Molecular Calculations. IV. Calculation of Static Electrical Response Properties. *J. Chem. Phys.* **1994**, *100*, 2975–2988.

(53) Frisch, M. J. et al. Gaussian 09 Revision D.01. Gaussian Inc. Wallingford CT 2009.

(54) Wiebke, J.; Moritz, A.; Cao, X.; Dolg, M. Approaching actinide(+III) hydration from first principles. *Phys. Chem. Chem. Phys.* **2007**, *9*, 459–465.

(55) Helm, L.; Merbach, A. Inorganic and Bioinorganic Solvent Exchange Mechanisms. *Chem. Rev.* **2005**, *105*, 1923–1960.

(56) Bayly, C. I.; Cieplak, P.; Cornell, W.; Kollman, P. A. A Well-Behaved Electrostatic Potential Based Method Using Charge Restraints for Deriving Atomic Charges: The RESP Model. *J. Phys. Chem.* **1993**, *97*, 10269–10280.

(57) Miertuš, S.; Scrocco, E.; Tomasi, J. Electrostatic Interaction of a Solute With a Continuum. a Direct Utilization of Ab Initio Molecular Potentials for the Prevision of Solvent Effects. *Chem. Phys.* **1981**, *55*, 117–129.

(58) Cances, E.; Mennucci, B.; Tomasi, J. A New Integral Equation Formalism for the Polarizable Continuum Model: Theoretical Background and Applications to Isotropic and Anisotropic Dielectrics. *J. Chem. Phys.*. **1997**, *107*, 3032–3041.

(59) Jorgensen, W. L.; Chandrasekhar, J.; Madura, J. D.; Impey, R. W.; Klein, M. L. Comparison of Simple Potential Functions for Simulating Liquid Water. *J. Chem. Phys.* **1983**, *79*, 926–935.

(60) Todorov, I. T.; Smith, W.; Trachenko, K.; Dove, M. T. DL_POLY_3: New Dimensions in Molecular Dynamics Simulations Via Massive Parallelism. *J. Mat. Chem.* **2006**, *16*, 1911–1918.

(61) Fourest, B.; Duplessis, J.; David, F. Comparison of Diffusion Coefficients and Hydrated Radii for some Trivalent Lanthanide and Actinide Ions in Aqueous Solution. *Radiochim. Acta* **1984**, *36*, 191–195.

(62) Martelli, F.; Abadie, S.; Simonin, J.-P.; Vuilleumier, R.; Spezia, R. Lanthanoids(III) and actinoids(III) in water: Diffusion coefficients and hydration enthalpies from polarizable molecular dynamics simulations. *Pure Appl. Chem.* **2013**, *85*, 237–246.

(63) Marcus, Y.; Loewenschuss, A. Standard Thermodynamic Functions of the Gaseous Actinyl Ions MO_2^{n+} and for Their Hydration. *J. Chem. Soc. Faraday Trans.* **1986**, *82*, 2873–2886.

(64) Gibson, J. K.; Haire, R. G.; Santos, M.; Maralo, J.; Pires de Matos, A. Oxidation Studies of Dipositive Actinide Ions, An^{2+} (An = Th, U, Np, Pu, Am) in the Gas Phase: Synthesis and Characterization of the Isolated Uranyl, Neptunyl, and Plutonyl Ions UO_2^{2+}(g), NpO_2^{2+}(g) and PuO_2^{2+}(g). *J. Phys. Chem. A* **2005**, *109*, 2768–2781.

(65) Yeh, I.-C.; Hummer, G. System-Size Dependence of Diffusion Coefficients and Viscosities from Molecular Dynamics Simulations with Periodic Boundary Conditions. *J. Phys. Chem. B* **2004**, *108*, 15873–15879.

(66) Ankudinov, A. L.; Nesvizhskii, A. I.; Rehr, J. J. Dynamic Screening Effects in X-Ray Absorption Spectra. *Phys. Rev. B* **2003**, *67*, 115120.

(67) Rehr, J. J.; Albers, R. Theoretical Approaches to X-Ray Absorption Fine Structure. *Rev. Mod. Phys.* **2000**, *72*, 621–654.

(68) Conradson, S. D.; Clark, D. L.; Neu, M. P.; Runde, W. H.; Tait, C. D. Characterizing the Plutonium Aquo Ions by XAFS Spectroscopy. *Los Alamos Science* **2000**, *26*, 418–421.

(69) den Auwer, C.; Drot, R.; Simoni, E.; Conradson, S. D.; Gailhanou, M.; Mustre de Leon, J. Grazing Incidence XAFS Spectroscopy of Uranyl Sorbed Onto TiO2 Rutile Surfaces. *New J. Chem.* **2003**, *27*, 648–655.

(70) Runde, W. H.; Mincher, B. J. Recent Advances in Aqueous Actinide Chemistry and Thermodynamics. *Chem. Rev.* **2011**, *111*, 5726–5741.

Graphical TOC Entry

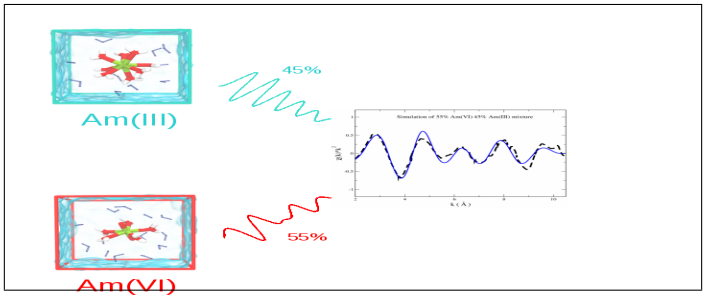

Understanding the experimental EXAFS spectrum of an Americium cation mixture in water by building the individual contributions theoretically.